# Backbendings of superdeformed bands in $^{36,40}$Ar *

Xu-Hui Xiang(向旭辉)† Xiao-Tao He(贺晓涛)†;1)

College of Material Science and Technology, Nanjing University of Aeronautics and Astronautics, Nanjing 210016, China

**Abstract:** Experimentally observed superdeformed (SD) rotational bands in $^{36}$Ar and $^{40}$Ar are studied by the cranked shell model (CSM) with the pairing correlations treated by a particle-number-conserving (PNC) method. This is the first time that PNC-CSM calculations have been performed on the light nuclear mass region around $A$=40. The experimental kinematic moments of inertia $J^{(1)}$ versus rotational frequency are reproduced well. The backbending of the SD band at frequency around $\hbar\omega$=1.5 MeV in $^{36}$Ar is attributed to the sharp rise of the simultaneous alignments of the neutron and proton $1d_{5/2}[202]5/2$ pairs and $1f_{7/2}[321]3/2$ pairs, which is a consequence of the band crossing between the $1d_{5/2}[202]5/2$ and $1f_{7/2}[321]3/2$ configuration states. The gentle upbending at low frequency of the SD band in $^{40}$Ar is mainly affected by the alignments of the neutron $1f_{7/2}[321]3/2$ pairs and proton $1d_{5/2}[202]5/2$ pairs. The PNC-CSM calculations show that besides the diagonal parts, the off-diagonal parts of the alignments play an important role in the rotational behavior of the SD bands.

**Keywords:** superdeformed band, backbending, moment of inertia, cranked shell model

**PACS:** 21.10.Re, 21.60.Cs, 23.20.Lv **DOI:** 10.1088/1674-1137/42/5/054105

## 1 Introduction

Since the first observation of the superdeformed rotational band in $^{152}$Dy [1], numerous superdeformed bands have been discovered in the "traditional" superdeformed regions of mass numbers 80,130,150 and 190. The latest superdeformed archipelago has been found in the light mass region around $A = 40$. High spin states of the superdeformed rotational bands have been successfully populated in experiment for $^{36}$Ar [2, 3], $^{40}$Ar [4], $^{40}$Ca [5] and $^{44}$Ti [6]. Most interestingly, these nuclei are magic or near-magic systems, whose ground states correspond to a spherical shape. This exotic shape coexistence phenomenon provides an ideal test ground for theoretical models.

Many microscopic descriptions of these bands have been given, including cranked Nilsson-Strutinsky (CNS) [2], shell model (SM) [2, 7–9], cranked relativistic mean-field (CRMF) [5], Hartree-Fock BCS with Skyrme interaction SLy6 [10], angular momentum projected generator coordinate (AMP-GCM) method with the Gogny force D1S [11], projected shell model (PSM) [12, 13], multidimensionally constrained relativistic mean field (MDC-RMF) [14], antisymmetrized molecular dynamics (AMD) [15–18], cluster models [19], cranked Hartree-Fock-Bogoliubov (CHFB) [4] and so on. Each of these models can give a good description of certain aspects of these superdeformed nuclei under certain assumptions. Therefore, comprehensive understanding of the superdeformed nuclear structure of these magic or near-magic nuclei needs complementary investigations of different models. Among these models, as stated in Refs. [8, 9], the interacting shell model, when affordable, is a prime choice. However, to carry out practical shell model calculations of $^{36}$Ar, the $1d_{5/2}$ orbital has to be excluded from the *sd-pf* shell space [2]. Recently, shell model calculations were performed on $^{46}$Ti, where a limited configuration space consisting of $1d_{3/2}$ and $1f_{7/2}$ orbitals was constructed, but the full *sd-pf* calculations are still not possible [20]. Therefore, as the full *sd-pf* shell model calculations are still difficult in the $A$=40 mass region, it is necessary to test an efficient shell model truncation scheme for well-deformed nuclei in the light mass region.

The cranked shell model has been proved to be a powerful tool to study the nuclear collective rotation of most areas in the nuclear chart. However, until now no cranked shell model calculation has been performed on the SD bands around the $A$ = 40 region. For the first time, we perform cranked shell model calculations with the pairing treated by the particle-number conserving (PNC-CSM) method on the SD bands in such a light nuclear mass region. The PNC-CSM method is pro-

Received 23 February 2018, Published online 13 April 2018

∗ Supported by National Natural Science Foundation of China (11775112 and 11275098) and the Priority Academic Program Development of Jiangsu Higher Education Institutions

1) E-mail: hext@nuaa.edu.cn

† These authors contributed equally to this paper.

posed to treat the pairing correlations and blocking effects properly. It has previously been applied successfully to describe the properties of normal deformed nuclei in the $A\sim170$ mass region [21–26], superdeformed nuclei in the $A\sim150$, 190 mass regions [27–31], high-K isomeric states in the rare-earth and actinide mass region [32–35], and recently in the heaviest actinides and light superheavy nuclei around the $Z\sim100$ region [36–41]. Most recently, the PNC method, referred to as the "shell-model-like approach" (SLAP) in Ref. [42], was implemented to treat the cranking many-body Hamiltonian based on covariant density functional theory including pairing correlations with exact particle number conservation [43]. In contrast to the Bardeen-Cooper-Schrieffer (BCS) or Hartree-Fock-Bogolyubov (HFB) approaches, the cranked shell model Hamiltonian is diagonalized directly in a truncated Fock space in the PNC method [44, 45]. Therefore, particle number is conserved and Pauli blocking effects are taken into account exactly.

In the present work we focus on the case of $^{36}$Ar and its heavier isotope $^{40}$Ar, of which superdeformed rotational bands have been established up to high spin. The present PNC-CSM calculations can reproduce the experimentally extracted moments of inertia within an acceptable deviation. This indicates that the PNC-CSM method is a promising approach in the description of light rotational nuclei. The observed backbendings of the rotational bands can be understood in the PNC-CSM framework as the band crossing between the [321]3/2 and [202]5/2 configuration bands for both the neutron and proton. Note that the Nilsson [321]3/2 and [202]5/2 levels stem from the spherical $1f_{7/2}$ and $1d_{5/2}$ orbitals, respectively. Therefore the effect of the $1d_{5/2}$ orbital on these rotational SD bands is non-trivial .

## 2 Theoretical framework

The cranked shell model Hamiltonian of an axially symmetric nucleus in the rotating frame reads,

$$H_{\rm CSM}=\sum_{\rm n}(h_{\rm Nil}-\omega j_x)_{\rm n}+H_{\rm P}, \tag{1}$$

where $h_0(\omega)=h_{\rm Nil}-\omega j_x$ is the single-particle part with $h_{\rm Nil}$ being the Nilsson Hamiltonian [46, 47] and $-\omega j_x$ being the Coriolis force with the cranking frequency $\omega$ about the $x$ axis. The cranked Nilsson orbitals are obtained by diagonalizing the single-particle Hamiltonian $h_0(\omega)=h_{\rm Nil}-\omega j_x$.

The pairing $H_{\rm P}$ includes monopole and quadrupole pairing correlations,

$$H_{\rm P}(0) = -G_0\sum_{\xi\eta}a^\dagger_\xi a^\dagger_{\overline{\xi}}a_{\overline{\eta}}a_\eta\ , \tag{2}$$

$$H_{\rm P}(2) = -G_2\sum_{\xi\eta}q_2(\xi)q_2(\eta)a^\dagger_\xi a^\dagger_{\overline{\xi}}a_{\overline{\eta}}a_\eta\ , \tag{3}$$

where $\overline{\xi}$ and $\overline{\eta}$ are the time-reversal states of the Nilsson states $\xi$ and $\eta$, respectively. The quantity $q_2(\xi)=\sqrt{16\pi/5}\langle\xi|r^2Y_{20}|\xi\rangle$ is the diagonal element of the stretched quadrupole operator. The corresponding effective pairing strengths $G_0$ and $G_2$ are connected with the dimension of the truncated cranked many-particle configuration (CMPC) space [48] in which $H_{\rm CSM}$ is diagonalized. In the following calculations, the CMPC space for $^{36,40}$Ar is constructed in the $N=0\sim4$ major shells for both neutrons and protons. By taking the CMPC truncation (Fock space truncation), the dimensions of the CMPC space are about 500, and the corresponding effective monopole and quadrupole pairing strengths are $G_{0p}=G_{0n}=0.18$ MeV and $G_{2p}=G_{2n}=0.08$ MeV, respectively. The yrast and low-lying eigenstates are obtained as,

$$|\psi\rangle=\sum_i C_i|i\rangle\ , \tag{4}$$

where $|i\rangle$ is a cranked many-particle configuration and $C_i$ is the corresponding probability amplitude.

The angular momentum alignment $\langle J_x\rangle$ of the state $|\psi\rangle$ is,

$$\langle\psi|J_x|\psi\rangle=\sum_i|C_i|^2\langle i|J_x|i\rangle+2\sum_{i<j}C^*_iC_j\langle i|J_x|j\rangle. \tag{5}$$

Since $J_x$ is an one-body operator, the matrix element $\langle i|J_x|j\rangle$ is nonzero only when $|i\rangle$ and $|j\rangle$ differ by one particle occupation, which are denoted by orbitals $\mu$ and $\nu$. Then $|i\rangle=(-)^{M_{i\mu}}|\mu\cdots\rangle$ and $|j\rangle=(-)^{M_{j\nu}}|\nu\cdots\rangle$ with the ellipsis stands for the same particle occupation and $(-)^{M_{i\mu}}=\pm1$ and $(-)^{M_{j\nu}}=\pm1$ according to whether the permutation is even or odd. The angular momentum alignment can be expressed as the diagonal and the off-diagonal parts,

$$\begin{aligned}\langle J_x\rangle &= \langle J_x(\mu)\rangle+\langle J_x(\mu\nu)\rangle\\ &= \sum_\mu j_x(\mu)+\sum_{\mu<\nu}j_x(\mu\nu).\end{aligned} \tag{6}$$

The kinematic moment of inertia is given by $J^{(1)}=\langle\psi|J_x|\psi\rangle/\omega$. For the details of the PNC-CSM method, see Refs. [21, 44, 45].

## 3 Calculation and discussion

The Nilsson parameters $(\kappa,\mu)$ are taken from Ref. [49]. Since $^{36}$Ar is a $N=Z$ symmetric nuclear system and the density of the single-particle level is low, the same set of $(\kappa,\mu)$ (values for protons in Ref. [49]) is used for neutrons and protons in the present calculations. Although there are four more neutrons in $^{40}$Ar, using different sets of $(\kappa,\mu)$ for neutrons and protons (values in Ref. [49]) gives very similar results within 0.1 $\hbar^2$MeV$^{-1}$ shift of moment of inertia. Therefore, the same set of $(\kappa,\mu)$ is adopted for $^{40}$Ar as well. To reproduce

the experimental backbending of the SD band in $^{36}$Ar, the values of ($\kappa_2$,$\kappa_3$) are modified from (0.105,0.090) to (0.080,0.120), respectively. If the original values of (0.105,0.090) are used, the band crossing would appear around the quadrupole deformation $\varepsilon_2$=0.6, rather than the most predicted deformation around $\varepsilon_2 = 0.5$. The corresponding Nilsson diagram for protons or neutrons is shown in Fig. 1. It shows that the deformed $N=Z=18$ and 20 energy gaps appear at the well-deformed prolate region around $\varepsilon_2 = 0.4$ and 0.5, respectively. At the oblate deformation side, the $N=Z=20$ energy gap around $\varepsilon_2=-0.4$ is as large as the spherical shell gap at $N=Z=20$.

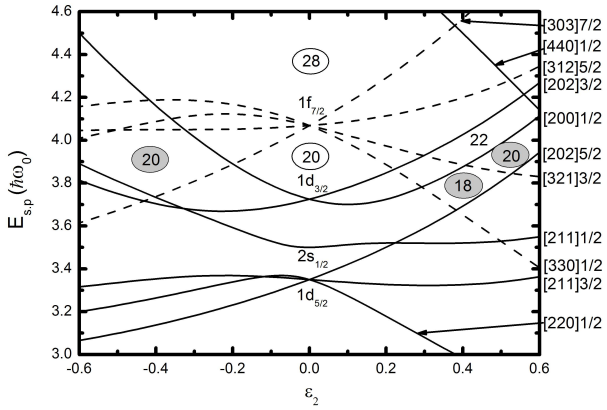


Fig. 1. The Nilsson diagram for protons or neutrons around $N = Z = 20$ with quadrupole deformation $\varepsilon_2$ ($\varepsilon_4 = 0$ and $\varepsilon_6 = 0$.). The Nilsson parameters ($\kappa$,$\mu$) are taken from Ref. [49]. The $\kappa_2$,$\kappa_3$ are modified slightly as $\kappa_2$=0.08,$\kappa_3$=0.12.

The quadrupole deformation $\beta_2 = 0.45$ was suggested by cranked Nilsson-Strutinsky calculations for the SD bands of $^{36}$Ar in the original experimental paper [2]. Later, a large low spin quadrupole deformation $\beta_2$=0.46±0.03 was deduced from the $B$(E2) value for the $4^+ \to 2^+$ SD transition in Ref. [3]. For $^{40}$Ar, the observed superdeformed structure was calculated by the cranked Hartree-Fock-Bogoliubov method with the $P$+$QQ$ force [4]. The calculation shows that $\beta_2$=0.57 at $I=0\hbar$ and the deformation gradually decreases to 0.45 at $I$=12$\hbar$. Triaxiality is found to be almost zero ($\gamma\approx0^\circ$) throughout this angular momentum range. Calculations by the parity and angular momentum projection and the generator coordinate method suggest a quadrupole deformation $\beta_2 = 0.478$ and triaxial deformation with $\gamma \approx 10^\circ$ [18]. In the PNC-CSM frame, the nucleus is restricted to an axial symmetric shape in the whole spin range with the fixed deformation parameters. $\varepsilon_2$=0.48 and $\varepsilon_2$=0.5 are adopted for $^{36}$Ar and $^{40}$Ar, respectively. For $^{36}$Ar, present calculations show that including the higher order axial symmetric deformations, whose values are taken as $\varepsilon_4 = 0.06$ and $\varepsilon_6 = -0.06$, leads to a sharper backbending around $\hbar\omega = 1.5$ MeV of the SD band, which reproduces the experimental backbending better than zero $\varepsilon_4$ and $\varepsilon_6$ results. However, the higher order deformations are neglected for the nuclei in the light mass region in the literature. How they affect the single-particle level structure and collective motion of the light mass nuclei need further systematic investigation.

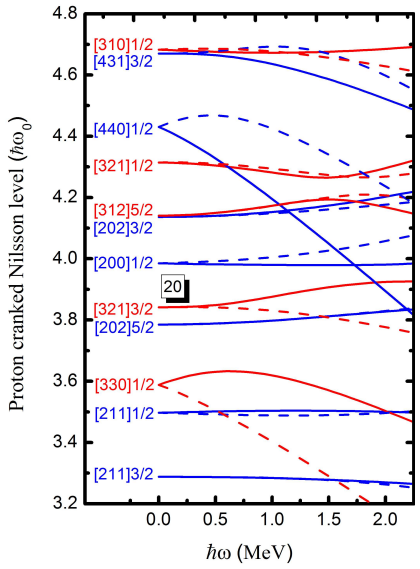


Fig. 2. (color online) Cranked proton Nilsson levels near the Fermi surface of $^{36}$Ar with deformation parameter $\varepsilon_2$=0.48, $\varepsilon_4$=0.06, $\varepsilon_6$=−0.06. The signature $\alpha$=+1/2 ($\alpha$=−1/2) levels are denoted by solid (dashed) lines. The positive (negative) parity levels are denoted by blue (red) lines. Cranked neutron Nilsson levels are the same.

With the above selected parameters, the cranked Nilsson levels for $^{36}$Ar are calculated as shown in Fig. 2. The results are the same for neutrons and protons. The proton/neutron Fermi surface of $^{36}$Ar is located between the $1f_{7/2}[321]3/2$ and $1d_{5/2}[202]5/2$ orbitals. Since these two Nilsson orbitals stay close to each other and cross around $\hbar\omega = 1.5$ MeV ($\alpha = -1/2$), a band crossing is likely to arise around $\hbar\omega = 1.5$ MeV. In contrast, the neutron Fermi surface of $^{40}$Ar is lifted up to the deformed shell gap at $N$=22 where the band crossing occurs between the $1d_{3/2}[200]1/2$ and $1g_{9/2}[440]1/2$ orbitals around $\hbar\omega$=1.5 MeV. Since the $1g_{9/2}[440]1/2$ orbital is a high−$j$ low−$\Omega$ intruder orbital, which is characterized by its large contributions to alignment and large Coriolis responses, a sharp backbending would arise around $\hbar\omega$=1.5 MeV. However, the experimentally observed SD band in $^{40}$Ar is up to spin $I^\pi = 12^+$, which is equivalent to $\hbar\omega = 1.35$ MeV. The predicted band crossing would then occur beyond the experimentally observed frequency range. Therefore, we will not discuss it here.

The comparison of the theoretical $J^{(1)}$ with the extracted experimental values for SD bands in $^{36,40}$Ar is

plotted in Fig. 3. The near-perfect rotational behavior of $^{36}$Ar was observed in experiment up to spin $I=10\hbar$ (around rotational frequency $\hbar\omega=1.5$ MeV) where a backbending arises [2]. The agreement of the backbending frequency around $\hbar\omega$=1.5 MeV is remarkably good. The calculated backbending of $J^{(1)}$ at $\hbar\omega>1.5$ MeV is less pronounced than the experimental data. The cranked Nilsson-Strutinsky calculation shows the system maintains an axially symmetric shape before the backbending while it changes shape to have triaxial deformation after the backbending [3]. The cranked Skyrme-Hartree-Fock calculation reveals that the shape of the superdeformed $^{36}$Ar system becomes triaxial and evolves toward an oblate shape at high spin limit. The PNC-CSM calculation is carried out with fixed symmetric deformations throughout the whole frequency range. To develop the present model to take into account the shape evolution may improve quantitive agreement between theoretical results and experimental data.

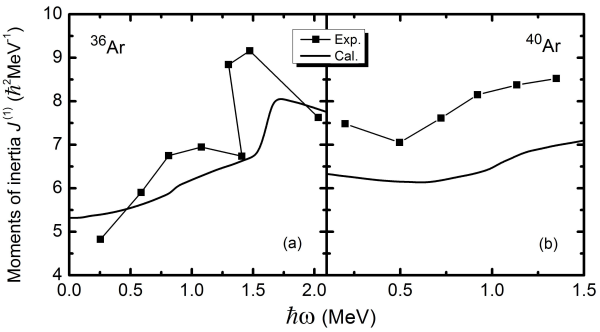


Fig. 3. Comparison of the experimental kinematic moment of inertia $J^{(1)}$ of the SD bands in $^{36}$Ar (a) and $^{40}$Ar (b) with the PNC-CSM calculations. Experimental data are denoted by solid squares and theoretical results are denoted by solid lines.

To reveal the microscopic mechanism of the backbending of the rotational band is often of interest in theoretical studies, since it can provide valuable information to help understand the microscopic structures of the rotating nuclear system more deeply. Based on the analysis of projected shell model calculations, the backbending of the SD band in $^{36}$Ar is explained as the result of the 0-, 2-, and 4-quasiparticle (qp) bands crossing each other at the same angular momentum $I^+=10^+$ [12].

In the PNC-CSM calculations, the band crossing in $^{36}$Ar is clearly shown by the occupation probabilities $n_\mu$ of each cranked Nilsson orbital $\mu$ in Fig. 4(a) and 4(c). We can see that the $n_\mu$ of neutrons and protons are the same. Before the backbending (at $\hbar\omega\leq1.5$ MeV), $1f_{7/2}[321]3/2$, the orbital just above the Fermi surface, is almost empty ($n_\mu\approx0$) and $1d_{5/2}[202]5/2$, the orbital just below the Fermi surface, is almost fully occupied ($n_\mu\approx2$). This switches round after the backbending. Therefore, the backbending results from the simultaneous band crossing of neutrons and protons between the ground state (0-qp) band and the $1f_{7/2}[321]3/2$ (with signature $\alpha=\pm1/2$) configuration state (4-qp) band. This is consistent with the conclusion of projected shell model calculations. Furthermore, the PNC-CSM calculations present clearly why, in contrast to the common band crossing picture, the 2-qp configurations do not have a chance to play a major role in the structure of the SD yrast band in $^{36}$Ar. Since $^{36}$Ar is a $N=Z$ symmetric nucleus, the neutron and proton signature pairs are excited from $1d_{5/2}[202]5/2$ to $1f_{7/2}[321]3/2$ configuration state simultaneously to form a 4-qp state immediately after the backbending.

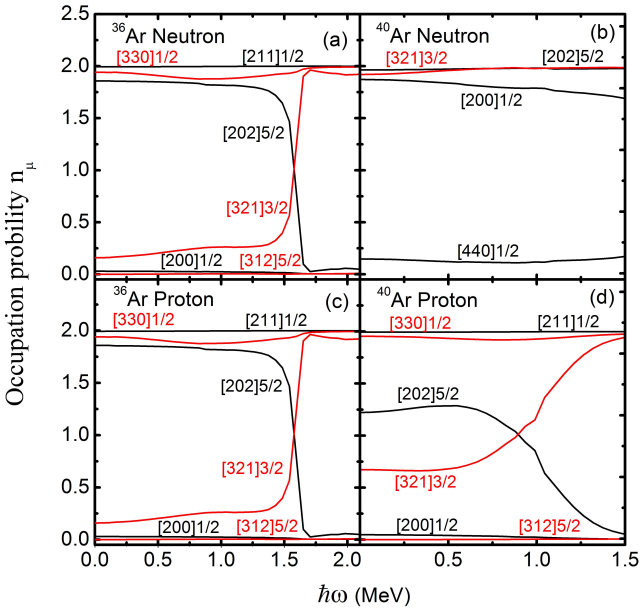


Fig. 4. (color online) Occupation probability $n_\mu$ of each orbital $\mu$ (including both $\alpha=\pm1/2$) near the Fermi surface for SD bands in $^{36}$Ar (left) and $^{40}$Ar (right). The $n_\mu$ of the positive (negative) parity levels are denoted by black (red) lines.

To quantify the effect, more detailed information on the angular momentum alignment $\langle J_x(\mu)\rangle$ from each single particle orbital $\mu$ and the interference $\langle J_x(\mu\nu)\rangle$ between orbitals $\mu$ and $\nu$ are presented in Fig. 5. As shown in Fig. 5(a) and 5(c), the sharp rise of $J^{(1)}$ in $^{36}$Ar mainly results from the contribution of the sudden increased simultaneous alignments of neutron and proton $1d_{5/2}[202]5/2$ pairs and $1f_{7/2}[321]3/2$ pairs at $\hbar\omega=1.5$ MeV. Besides, their involved interference terms are important too. While $\langle J_x([321]1/2\otimes[321]3/2)\rangle$ decreases suddenly at $\hbar\omega$=1.5 MeV, $\langle J_x([330]1/2\otimes[321]3/2)\rangle$ shows an excessive sharp increase. The smooth rise of $J^{(1)}$ at low frequency is mainly attributed to the gradual alignments of neutron and proton $1f_{7/2}[330]1/2$ pairs and $1d_{5/2}[220]1/2$ pairs.

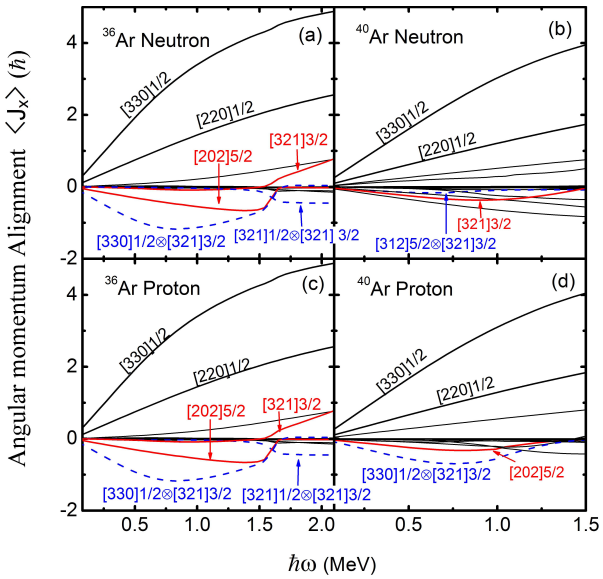


Fig. 5. (color online) The direct contributions to the angular momentum alignment $\langle J_x\rangle$ from the particle occupying the cranked orbital $\mu$ (denoted by solid lines) and the interference $\langle J_x(\mu\nu)\rangle$ between orbital $\mu$ and $\nu$ (denoted by the dashed lines) for the SD band of $^{36}$Ar (left) and $^{40}$Ar (right).

The rotational behavior of the SD band in $^{40}$Ar is quite different. Only a slight upbending of $J^{(1)}$ appears at low spin (around $\hbar\omega$=0.5 MeV). Then $J^{(1)}$ increases smoothly with rotational frequency. The PNC-CSM calculations reproduce the experimental variation tendency very well. However, the theoretical results underestimate the data by about 1.2 $\hbar^2$MeV$^{-1}$ throughout the whole observed frequency range. The n-p pairing would be important in such a (near-)symmetric nuclear system, but is not included in the present PNC-CSM method. This could be one of the reasons for the systematic shift down of the theoretical results. Nevertheless, further investigations aimed at the effect of the n-p pairing should be fulfilled by the PNC-CSM method in this mass region.

Due to the four additional neutrons in $^{40}$Ar, the rotational behavior differs a lot from that of $^{36}$Ar. From the occupation probabilities in Fig. 4(b), we can see that the $1d_{3/2}[200]1/2$ and $1f_{7/2}[321]3/2$ orbitals are fully occupied ($n_\mu \approx 2$). Since the deformed $N=22$ shell gap is comparatively big, there is no neutron band crossing over the experimentally observed frequency range. The proton occupation probabilities [see Fig. 4(d)] vary accordingly because of the change of the mean field. The $1d_{5/2}[202]5/2$ orbital is more than half occupied ($n_\mu \approx 1.25$), and the $1f_{7/2}[321]3/2$ orbital is less than half occupied ($n_\mu \approx 0.75$). From Fig. 5(b) and 5(d), the slight upbending at the low frequency is mainly attributed to the alignments of the neutron $1f_{7/2}[321]3/2$ pairs and proton $1d_{5/2}[202]5/2$ pairs, and their involved interference terms of neutron $\langle J_x([312]5/2\otimes[321]3/2)\rangle$ and proton $\langle J_x([330]1/2\otimes[321]3/2)\rangle$.

## 4 Conclusions

For the first time, the cranked shell model with the pairing correlations treated by the particle-number-conserving method has been used to describe the superdeformed rotational bands in the $A$=40 mass region. The calculations are carried out within $N=0\sim4$ major shells, with axially symmetric deformation parameters $\varepsilon_{2,4,6}$ being considered and the pairing correlations being treated properly. The experimental kinematic moments of inertia $J^{(1)}$ versus rotational frequency in $^{36}$Ar and $^{40}$Ar are reproduced well. This may convince us that the PNC-CSM method is an efficient method to describe the rotational properties of the superdeformed nuclei around the $A$=40 mass region.

The microscopic mechanism of the variation of the superdeformed bands versus frequency is explicit in the PNC-CSM calculations. The backbending around $\hbar\omega$= 1.5 MeV of the SD band in $^{36}$Ar is clearly presented by analysis of the dominant components of the total wave function of the cranked shell model Hamiltonian. It is attributed to the simultaneous alignments of neutron and proton $1d_{5/2}[202]5/2$ pairs and $1f_{7/2}[321]3/2$ pairs, which is caused by the band crossing between the $1d_{5/2}[202]5/2$ and $1f_{7/2}[321]3/2$ configuration states. As for $^{40}$Ar, four more additional neutrons raise the neutron Fermi surface to the $N$=22 deformed shell gap. There is no band crossing over the experimentally observed frequency range. Therefore, the variation of the $J^{(1)}$ versus frequency is much gentler. The slight upbending at low frequency is mainly caused by the alignments of the neutron $1f_{7/2}[321]3/2$ pairs and proton $1d_{5/2}[202]5/2$ pairs. Moreover, the PNC-CSM results show that besides the diagonal parts, the off-diagonal parts are very important. We see that not only the $1f_{7/2}$ orbital, but also $1d_{5/2}$ plays a very important role in the rotational behavior of the SD bands in $^{36,40}$Ar, which cannot be neglected.

## References


1 P. J. Twin, B. M. Nyakó, A. H. Nelson et al, Phys. Rev. Lett., **57**(7): 811–814 (1986)
2 C. E. Svensson, A. O. Macchiavelli, A. Juodagalvis et al, Phys. Rev. Lett., **85**(13): 2693–2696 (2000)
3 C. E. Svensson, A. O. Macchiavelli, A. Juodagalvis et al, Phys. Rev. C, **63**(6): 061301 (2001)
4 E. Ideguchi, S. Ota, T. Morikawa et al, Phys. Lett. B, **686**(1): 18–22 (2010)

5 E. Ideguchi, D. G. Sarantites, W. Reviol et al, Phys. Rev. Lett., **87**(22): 222501 (2001)
6 C. D. O'Leary, M. A. Bentley, B. A. Brown et al, Phys. Rev. C, **61**(6): 064314 (2000)
7 A. Poves, Nucl. Phys. A, **731**: 339–346 (2004)
8 E. Caurier, F. Nowacki, and A. Poves, Phys. Rev. Lett., **95**(4): 042502 (2005)
9 E. Caurier, J. Menéndez, F. Nowacki et al, Phys. Rev. C, **75**(5): 054317 (2007)
10 M. Bender, H. Flocard, and P. H. Heenen, Phys. Rev. C, **68**(4): 044321 (2003)
11 R. R. Rodríguez-guzmán, J. L. Egido, and L. M. Robledo, Int. J. Mod. Phys. E, **13**(01): 139–146 (2004)
12 G. L. Long and Y. Sun, Phys. Rev. C, **63**(2): 021305(R) (2001)
13 Y. C. Yang, Y. X. Liu, Y. Sun et al, arXiv: 1508.04055
14 B. N. Lu, E. Hiyama, H. Sagawa et al, Phys. Rev. C, **89**(4): 044307 (2014)
15 Y. Kanada-En'yo and M. Kimura, Phys. Rev. C, **72**(6): 064322 (2005)
16 M. Kimura and H. Horiuchi, Nucl. Phys. A, **767**: 58–80 (2006)
17 Y. Taniguchi, M. Kimura, Y. Kanada-En'yo et al, Phys. Rev. C, **76**(4): 044317 (2007)
18 Y. Taniguchi, Y. Kanada-En'yo, M. Kimura et al, Phys. Rev. C, **82**(1): 011302 (2010)
19 T. Sakuda and S. Ohkubo, Nucl. Phys. A, **744**: 77–91 (2004)
20 N. H. Medina, J. R. B. Oliveira, F. Brandolini et al, Phys. Rev. C, **84**(2): 024315 (2011)
21 J. Y. Zeng, T. H. Jin, and Z. J. Zhao, Phys. Rev. C, **50**(3): 1388–1397 (1994)
22 C. S. Wu and J. Y. Zeng, Phys. Rev. C, **44**(6): 2566–2580 (1991)
23 J. Y. Zeng, S. X. Liu, L. X. Gong et al, Phys. Rev. C, **65**(4): 044307 (2002)
24 S. X. Liu, J. Y. Zeng, Phys. Rev. C, **66**(6): 067301 (2002)
25 S. X. Liu, J. Y. Zeng, and L. Yu, Nucl. Phys. A, **735**(1): 77–85 (2004)
26 J. Y. Zeng, S. X. Liu, Y. A. Lei et al, Phys. Rev. C, **63**(2): 024305 (2001)
27 C. S. Wu, L. Cheng, C. Z. Lin et al, Phys. Rev. C, **45**(5): 2507–2510 (1992)
28 S. X. Liu, J. Y. Zeng, and E. G. Zhao, Phys. Rev. C, **66**(2): 024320 (2002)
29 S. X. Liu and J. Y. Zeng, Nucl. Phys. A, **736**(3-4): 269–279 (2004)
30 J. Y. Zeng, J. Meng, C. S. Wu et al, Phys. Rev. C, **44**(5): R1745–R1748 (1991)
31 X. T. He, S. Y. Yu, J. Y. Zeng et al, Nucl. Phys. A, **760**(3): 263–273 (2005)
32 B. H. Li, Z. H. Zhang, and Y. A. Lei, Chin. Phys. C, **37**(1): 014101 (2013)
33 Z. H. Zhang, Y. A. Lei, and J. Y. Zeng, Phys. Rev. C, **80**(3): 034313 (2009)
34 Z. H. Zhang, X. Wu, Y. A. Lei et al, Nucl. Phys. A, **816**(1-4): 19–32 (2009)
35 X. M. Fu, F. R. Xu, J. C. Pei et al, Phys. Rev. C, **87**(4): 044319 (2013)
36 Y. C. Li, X. T. He, Sci. Chin. Phys. Mech., **59**(7): 672011 (2016)
37 Z. H. Zhang, Sci. Chin. Phys. Mech., **59**(7): 672012 (2016)
38 Z. H. Zhang, J. Meng, E. G. Zhao et al, Phys. Rev. C, **87**(5): 054308 (2013)
39 Z. H. Zhang, X. T. He, J. Y. Zeng et al, Phys. Rev. C, **85**(1): 014324 (2012)
40 Z. H. Zhang, J. Y. Zeng, E. G. Zhao et al, Phys. Rev. C, **83**(1): 011304(R) (2011)
41 X. T. He, Z. Z. Ren, S. X. Liu et al, Nucl. Phys. A, **817**(1): 45–60 (2009)
42 J. Meng, J. Y. Guo, L. Liu et al, Front. Phy. China, **1**(1): 38–46 (2006)
43 Z. Shi, Z. H. Zhang, Q. B. Chen et al, Phys. Rev. C, **97**(3): 034317 (2018)
44 J. Y. Zeng, Y. A. Lei, T. H. Jin et al, Phys. Rev. C, **50**(2): 746–756 (1994)
45 J. Y. Zeng and T. S. Cheng, Nucl. Phys. A, **405**(1): 1–28 (1983)
46 S. Nilsson, Dan. Mat. Fys. Medd., **29**(16): 1–68 (1955)
47 S. Nilsson, C. F. Tsang, A. Sobiczewski et al, Nucl. Phys. A, **131**(1): 1–66 (1969)
48 C. S. Wu and J. Y. Zeng, Phys. Rev. C, **39**(2): 666–670 (1989)
49 T. Bengtsson and I. Ragnarsson, Nucl. Phys. A, **436**(1): 14–82 (1985)